

## Highlights

### **FlightKooba: A Fast Interpretable FTP Model**

Jing Lu, Xuan Wu, Yizhun Tian, Songhan Fan, Yali Fang

- A novel modeling method is proposed, achieving reduced time and memory overhead
- The method exhibits strong interpretability
- The model demonstrates excellent performance on multiple public datasets
- The study provides a new option for time series prediction

# FlightKooba: A Fast Interpretable FTP Model

Jing Lu<sup>a,b,\*</sup>, Xuan Wu<sup>a</sup>, Yizhun Tian<sup>a</sup>, Songhan Fan<sup>a</sup>, Yali Fang<sup>a</sup>

<sup>a</sup>*School of Computer Science, Civil Aviation Flight University of  
China, Guanghan, 618000, Sichuan, China*

<sup>b</sup>*College of Computer Science, Technology Nanjing University of Aeronautics and  
Astronautics Nanjing, Nanjing, 210000, Jiangsu, China*

---

## Abstract

The Koopman theory is a powerful and effective modeling tool for converting nonlinear systems into linear representations, and flight trajectory prediction (FTP) is a complex nonlinear system. However, current models applying the Koopman theory to FTP tasks are not very effective, model interpretability is indeed an issue, and the Koopman operators are computationally intensive, resulting in long training times. To address this issue, this paper proposes a new modeling and control framework based on the HIPPO method, the Koopman theory, and state space equations from cybernetics: FlightKooba. Inspired by the idea of structural state space equations, FlightKooba directly constructs the Koopman operators from data. This makes the framework highly interpretable and significantly reduces the number of trainable parameters in the module, thereby greatly reducing training time. Experiments have demonstrated the superiority of the FlightKooba modeling method in terms of time and memory consumption (training time comparable to the Mamba module without using CUDA-level acceleration; memory reduced by more than 50% on most datasets, with a tenfold reduction in the number of parameters), essentially completing the FTP task. It provides a new method for the fast computation of the Koopman operators, opening up new possibilities for the combination of time series forecasting and control.

*Keywords:* Flight trajectory prediction, Koopman, Mamba, SSM, Control

---

---

\*Corresponding author

*Email address:* `lujing_cafuc@nuaa.edu.cn` (Jing Lu )

## 1. Introduction

Flight trajectory prediction (FTP) is one of the fundamental research tasks in the field of aviation [6]. It is a key technology for various applications in the fields of flight operation quality assurance (FOQA) [4] and air traffic control (ATC) [33]. Flight trajectory prediction has always been an important aspect of air traffic management and safety. In flight training, trajectory prediction can be used to identify potential risks (such as attitude loss of control and altitude deviation) in advance by analyzing the trainee's operating habits and the aircraft's status (such as rudder deflection angle and roll rate). Flight trajectory prediction is not only a technical tool in training, but also a key factor in reshaping pilot training models. By integrating deep learning methods with physical models and combining real-time data-driven optimization strategies, we achieve comprehensive capability enhancements across the entire chain, from basic combat operations to tactical decision-making, driving the development of aviation training toward intelligence and precision. Currently, many scholars have introduced deep learning and neural networks to study flight trajectory prediction.

Deep learning methods have achieved relatively good success in modeling large complex systems using the [30] dataset. Existing deep learning technologies can be applied to various fields to predict time series data and achieve good results, such as weather forecasting [29] and traffic prediction [19].

The Koopman theory [17] has attracted increasing attention in recent years and has become a promising data-driven method. By representing nonlinear systems using linear state-space models (SSM) [16], Koopman operators can convert complex nonlinear dynamic systems into linear forms. Based on this method, Williams proposed an extended dynamic modal decomposition method (EDMD) to calculate the Koopman operator [31]. With the emergence and development of deep learning, Koopman theory has been combined with neural networks in many fields and has achieved great success in modeling many complex systems, such as probabilistic neural networks [14] and graph neural networks [20]. Although the prediction results of the above model are relatively accurate, it performs poorly in long sequence prediction tasks. Furthermore, neural network models themselves have a large number of parameters, and the current methods for calculating Koopman operators are time-consuming, which leads to enormous time consumption when combining the two methods.

To solve this problem, we turned our attention to the Mamba module, which is faster than the transformer module. In the Mamba structure, the core structure is similar to the linear SSM in Koopman theory. On this basis, features of recurrent neural networks (RNN) and convolutional neural networks (CNN) are integrated [7], which may also be the key to the success of the Mamba model. The core original form of this structure originates from polynomial approximation theory, namely HIPPO [8], which provides a certain theoretical basis for our discovery.

This paper proposes a time prediction model based on the HIPPO method, Koopman theory, and state space equations in cybernetics: FlightKooba. The HIPPO method was originally proposed to solve the problem of information compression in long sequences; Koopman theory solved the problem of analyzing and predicting nonlinear systems; and state space equations are mathematical tools for describing the behavior of dynamic systems. FlightKooba combines the three into one, which has great advantages in modeling complex nonlinear systems and is expected to solve the flight trajectory prediction (FTP) task. In addition, this method has a high level of interpretability that many network models lack, and it significantly reduces the number of parameters in the module, thereby greatly reducing the model training time: without a CUDA-level acceleration method, it achieves the same training time as the Mamba module. The contributions of this work are summarized as follows:

- We first proposed a data-driven unsupervised modeling method called FlightKooba, which uses state space equations to link the HIPPO method and Koopman theory for modeling complex nonlinear systems.
- We propose a new method for computing Koopman operators that significantly reduces the required computation time and is interpretable.
- We apply the model to a flight trajectory dataset (CAFUC) to test its performance in flight trajectory prediction (FTP) tasks and obtain effective results.
- We conducted experiments on other different time series datasets to validate the effectiveness and superiority of the model.

The remainder of this paper is organized as follows: Section 2 reviews the related work. Section 3 introduces FlightKooba for the FTP task. Section

4 presents the experiments, results, and visualizations. Finally, Section 5 concludes with a discussion of the findings and future work.

## 2. Related Works

Since its introduction, the Koopman operator theory [17] has been considered a powerful tool for analyzing dynamical systems. In the paper “Identification of MIMO Wiener-type Koopman models for data-driven model reduction using deep learning” [26], the scope of Koopman operator theory was extended to controlled systems, and some achievements were made in both modeling and control [34]. Similarly, when combined with neural network models, this new model with Koopman operators has achieved effective results in various fields such as robotics [27], fluid physics [23], and vehicle systems [5].

Although the Koopman model has received widespread attention, the current methods for solving Koopman operators can be broadly categorized into dynamic mode decomposition (DMD) [25] and its extensions (EDMD) [32], Hankel dynamic mode decomposition [2], spectral analysis, and computational methods using machine learning algorithms. For the first three data-driven methods, some computation is required to construct an approximation of the Koopman operator, which incurs additional time overhead. In contrast, our method can approximate the Koopman operator using polynomial approximation, thereby greatly reducing the time required to calculate the Koopman operator.

With the development of data-driven methods, models combining Koopman operators with neural networks have improved modeling accuracy and promoted the application of this model in various fields. In particular, in the field of learning control, various algorithms have been proposed to train corresponding control strategies in established models [10, 11, 12, 13]. There is also a new modeling method (MamKO) that combines the recently popular Mamba model with the Koopman operator [21].

We analyzed and learned from the history of the Mamba structure and discovered its predecessor: the HIPPO algorithm used in the SSM module of the structured state space sequence model (S4) [9]. It gives the SSM module a physical meaning: use a polynomial approximation of a time function and calculate the coefficient in front of each polynomial. Inspired by this method, we found that for the polynomial approximation equation of a certain function, we can use the idea of deriving state space equations from state

equations in “Principles of Automatic Control” to obtain the corresponding form of the Koopman operator. This is equivalent to directly deriving the approximate form of the Koopman operator from polynomial approximation, which greatly reduces the parameters of neural network calculations while ensuring a certain degree of accuracy.

### 3. Methodology

This section introduces FlightKooba, an explainable fast FTP model. Our approach is based on the HIPPO method for compressing continuous signals, Koopman theory for modeling complex systems, and state space equations to connect the two, resulting in FlightKooba. Here, we first provide a framework diagram of FlightKooba, and then explain each part in turn. As shown in Figure 1

#### 3.1. The Hippo Theory

In the paper “HiPPO: Recurrent Memory with Optimal Polynomial Projections,” the authors proposed the HiPPO theory, whose main idea is to use various polynomials to infinitely approximate a function in order to compress continuous information. After a series of deductions, the HIPPO algorithm ultimately arrives at an iterative formula for calculating the coefficient  $c_n$  in front of each polynomial. In this paper, we draw on this theoretical framework and select a Legendre polynomial with good performance as the first part of FlightKooba.

The value of  $c_n$  is related to the number of iterations, that is, it is related to time  $t$ . Let  $(c_0, c_1, \dots, c_n)$  be denoted as  $c_{t_k}$ , and the final result is:

$$c_{t_{k+1}} = \bar{N}c_{t_k} + \bar{M}\gamma_k \quad (1)$$

In the equation,  $t_k$  denotes the  $k$ th  $\delta_t$  time point.  $\gamma_k$  denotes the function value  $\gamma_{t_k}$  at time  $t_k$ . The matrices  $\bar{N}$  and  $\bar{M}$  are defined as follows:

$$\bar{N} = \left( I - \frac{\Delta t}{2} N \right)^{-1} \left( I + \frac{\Delta t}{2} N \right) \quad (2)$$

$$\bar{M} = \Delta t \left( I - \frac{\Delta t}{2} N \right)^{-1} M \quad (3)$$

Among them, the expressions of matrices  $N$  and  $M$  are related to the derivation of the HIPPO algorithm. In ”HiPPO: Recurrent Memory with

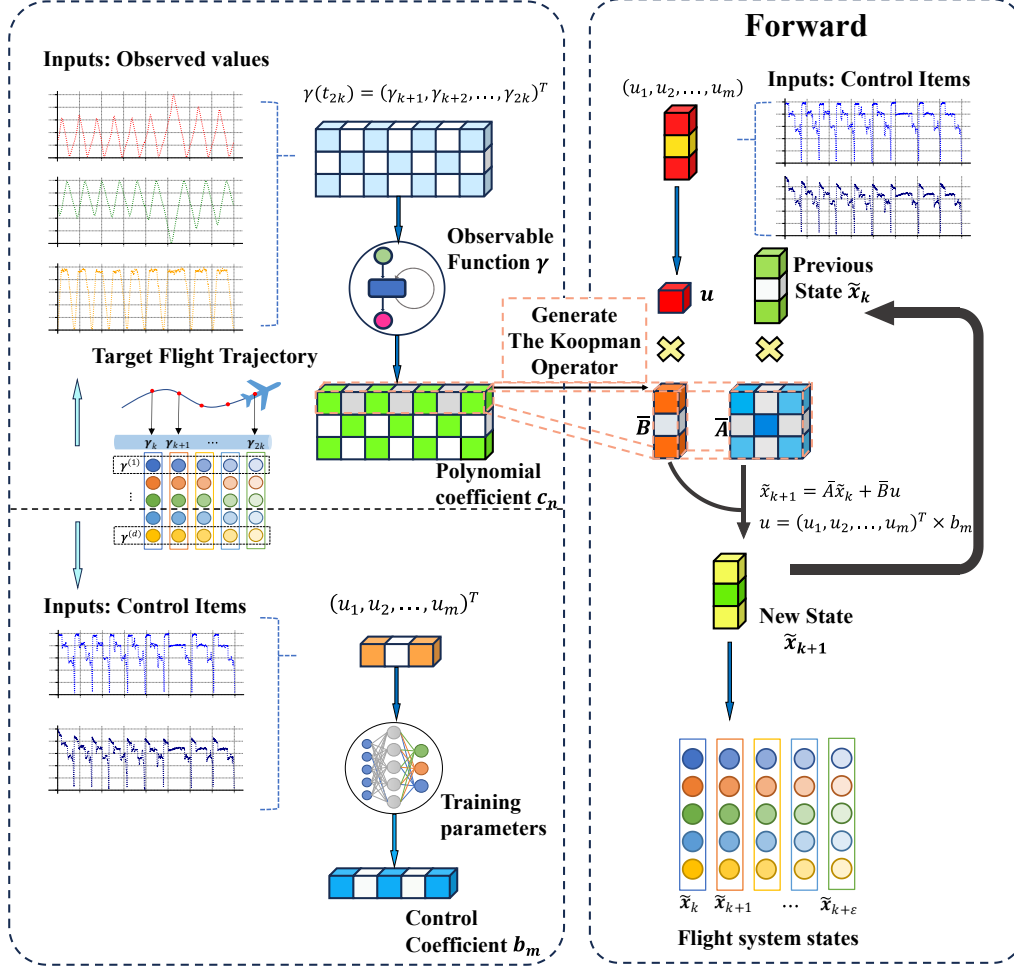


Figure 1: Structure of FlightKooba. FlightKooba consists of two parts: the first part calculates the coefficients corresponding to the polynomials that fit the system observation function; the second part generates the corresponding Koopman operators based on the results of the first part, which are used for subsequent prediction tasks.

Optimal Polynomial Projections” the expressions of matrices  $N$  and  $M$  corresponding to the two methods  $LegT$  and  $LegS$  are as follows:

$$(LegT)N_{n,k} = -\frac{1}{\omega} \begin{cases} \sqrt{(2n+1)(2k+1)}, & k < n \\ (-1)^{n-k} \sqrt{(2n+1)(2k+1)}, & k \geq n \end{cases} \quad (4)$$

$$(LegT)M_n = \frac{1}{\omega} \sqrt{2(2n+1)} \quad (5)$$

$$(LegS)N_{n,k} = - \begin{cases} \sqrt{(2n+1)(2k+1)}, & k < n \\ n+1, & k = n \\ 0, & k > n \end{cases} \quad (6)$$

$$(LegS)M_n = \sqrt{2(2n+1)} \quad (7)$$

In *LegT*,  $\omega$  denotes the length of the historical window of interest and is a hyperparameter. The difference between *LegT* and *LegS* is that *LegT* focuses more on information within a historical window length, while *LegS* focuses more on information across the entire time series length.

To speed up the calculation, we further derive equation 1, which yields:

$$c_{t_{2k+1}} = \overline{N}^{k-1} c_{t_k} + R \overline{M} \gamma(t_{2k}) \quad (8)$$

In the equation,  $R = (\overline{N}^{k-1}, \overline{N}^{k-2}, \dots, \overline{N}, I)$ .  $\gamma(t_{2k}) = (\gamma_{k+1}, \gamma_{k+2}, \dots, \gamma_{2k})^H$  represents the function value of the observed function starting from time  $2k$  and moving backward by  $k-1$  steps (a total of  $k$  values), i.e., a total of  $k$  iterations.

### 3.2. The Koopman Operator

The Koopman operator is an infinite-dimensional linear operator that can transform complex nonlinear dynamical systems into linear forms. It provides data-driven analytical tools for complex systems that lack explicit mathematical models, such as fluid dynamics, molecular dynamics, and complex networks. Its core idea is to characterize changes in the state of a system through the evolution of an observation function:

$$\mathcal{K}\varphi(x_t) = \varphi(x_{t+k}) \quad (9)$$

Here,  $\varphi$  denotes the observation function, and  $x_t$  denotes the value of state  $x$  at time  $t$ . The Koopman operator acts on  $\varphi$  to obtain the observation function of state  $x$  at time  $t+k$ . In the classic Koopman-based method, general time-invariant control of nonlinear systems is considered:

$$x_{k+1} = f(x_k, u_k) \quad (10)$$

In the equation,  $x_k$  is the state vector of the system at time  $k$ ;  $u_k$  is the input vector of the system at time  $k$ ;  $f$  is the nonlinear function describing



the dynamic behavior of the nonlinear system. According to the Koopman theory [17], the above equation can be expressed as:

$$\mathcal{K}\varphi(x_k, u_k) = \varphi \circ f(x_k, u_k) = \varphi(x_{k+1}) \quad (11)$$

Here,  $\varphi$  remains the observation function, and  $\circ$  denotes function composition. According to the design of the Koopman operator in [18], the system modeled by the Koopman operator in formula 9 can be described as:

$$z_{k+1} = Az_k + Bu_k \quad (12)$$

$$\hat{x}_k = Cz_k \quad (13)$$

Here,  $z_{k+1} = \varphi(x_k)$  represents the representation of the state vector  $x$  under the observation function, and the corresponding Koopman operators are divided into  $A$  and  $B$ . That is:

$$\mathcal{K} = \begin{bmatrix} A & B \\ * & * \end{bmatrix} \quad (14)$$

where  $\mathcal{K}$  is the Koopman operator, and  $*$  indicates that this part can be ignored or filled with zero.

### 3.3. Methods For Constructing State Space Equations

A state equation is a mathematical expression that describes the relationship between the state variables of the system. It is widely used in physics, chemistry, engineering (such as thermodynamics, fluid mechanics, control theory), and other fields to describe the laws governing the changes in the macroscopic properties of substances or systems as a function of state variables. In automatic control theory, state equations are usually differential equations based on physical laws (Newton's laws, Kirchhoff's laws).

State space equations are commonly used to describe linear dynamic systems, especially in control theory and systems engineering. They are mathematical expressions that describe how the state of a system changes over time. Take the simplest state equation as an example. The state equation of a spring-mass damping system is shown below:

$$F(t) = m\ddot{x} + c\dot{x} + kx \quad (15)$$

In the equation,  $m$  is the mass,  $k$  is the spring elasticity coefficient,  $c$  is the damping coefficient,  $x$  is the displacement,  $\dot{x}$  is the velocity, and  $\ddot{x}$  is the acceleration.

According to this equation, we can obtain:

$$\begin{cases} x = x_1 \\ \dot{x} = x_2 \\ \ddot{x} = -\frac{c}{m}x_2 - \frac{k}{m}x_1 + \frac{1}{m}F(t) \end{cases} \quad (16)$$

To describe the changes in the state vector of the system, we introduce  $X$  to represent the state vector, which can be expressed as follows:

$$\begin{cases} X = \begin{pmatrix} x_1 \\ x_2 \end{pmatrix} \\ \dot{X} = \begin{pmatrix} x_2 \\ -\frac{c}{m}x_2 - \frac{k}{m}x_1 + \frac{1}{m}F(t) \end{pmatrix} \end{cases} \quad (17)$$

Writing the above equation  $X$  in matrix form similar to 12, we obtain:

$$\dot{X} = AX + Bu \quad (18)$$

Among them:

$$\begin{cases} A = \begin{pmatrix} 0 & 1 \\ -\frac{k}{m} & -\frac{c}{m} \end{pmatrix} \\ B = \begin{pmatrix} 0 \\ \frac{1}{m} \end{pmatrix} \\ u = F(t) \end{cases} \quad (19)$$

The above two sets of equations give the general form of the state space equations for a spring-mass-damping system.

### 3.4. The Construction Method Of FlightKooba

In the previous three sections, we introduced the HIPPO method, the Koopman theory, and the construction of state space equations. Now we need to combine them.

In the HIPPO method, we obtain:

$$\gamma(t) = \sum_{i=0}^n c_n g_n(t) \quad (20)$$

In the equation,  $g_n$  is the normalized polynomial of the Legendre polynomial, and  $g_n$  satisfies the following relationship with  $p_n$  (where  $p_n$  is the Legendre polynomial):

$$g_n(t) = \sqrt{\frac{2n+1}{2}} p_n(t) \quad (21)$$

The Legendre polynomials have the following recursive formula:

$$\frac{d}{dt} p_n(t) = n p_{n-1}(t) \quad (22)$$

Substituting equations 21 and 22 into equation 20 yields:

$$\gamma(t) = \sqrt{\frac{1}{2}} c_0 p_0(t) + \sqrt{\frac{3}{2}} c_1 p_1(t) + \cdots + \sqrt{\frac{2n+1}{2}} c_n p_n(t) \quad (23)$$

$$= \sqrt{\frac{2n+1}{2}} c_n p_n(t) + \cdots + \sqrt{\frac{3}{2}} c_1 \frac{1}{n!} p_n'(t) + \sqrt{\frac{1}{2}} c_0 \frac{1}{n!} p_n^{(n)}(t) \quad (24)$$

That is, if we denote the coefficient  $\sqrt{\frac{2k+1}{2}} c_k \frac{1}{n(n-1)\dots(k+1)}$  as  $a_{n-k}$ , we obtain the following equation:

$$\gamma(t) = a_0 p_n(t) + a_1 p_n'(t) + \cdots + a_{n-1} p_n^{(n-1)}(t) + a_n p_n^{(n)}(t) \quad (25)$$

If we regard the Legendre polynomials  $p_n$  in the equation as the state of the system described by the equation under the observation function, then we can refer to the ideas in Section 3.3 to obtain the state variables:

$$x = \begin{bmatrix} x_1 = p_n \\ x_2 = p_n' \\ x_3 = p_n'' \\ \vdots \\ x_n = p_n^{(n-1)} \end{bmatrix} \quad (26)$$

$$\dot{x} = \begin{bmatrix} x_1' \\ x_2' \\ x_3' \\ \vdots \\ x_n' \end{bmatrix} = \begin{bmatrix} x_2 \\ x_3 \\ x_4 \\ \vdots \\ p_n^{(n)} \end{bmatrix} \quad (27)$$

The expression for  $p_n^{(n)}$  in the above equation can be derived from formula 25:

$$p_n^{(n)} = \frac{1}{a_n}(\gamma(t) - a_0x_1 - a_1x_2 - \dots - a_{n-1}x_n) \quad (28)$$

Substituting the above equation into formula 27 and writing it in matrix form similar to formula 18, we obtain:

$$\dot{x} = Ax + Bu \quad (29)$$

Among them, matrices  $A$  and  $B$  are respectively:

$$A = \begin{bmatrix} 0 & 1 & 0 & \dots & 0 \\ 0 & 0 & 1 & & 0 \\ \vdots & \vdots & \vdots & \ddots & \vdots \\ -\frac{a_0}{a_n} & -\frac{a_1}{a_n} & -\frac{a_2}{a_n} & \dots & -\frac{a_{n-1}}{a_n} \end{bmatrix} \quad (30)$$

$$B = \begin{bmatrix} 0 \\ 0 \\ \vdots \\ \frac{1}{a_n} \end{bmatrix} \quad (31)$$

where  $u$  is the value of  $\gamma$  at time  $t$ . If  $u$  consists of multiple terms, then we can obtain:

$$\gamma(t) = b_0u_0 + b_1u_1 + \dots + b_mu_m \quad (32)$$

The coefficients  $(b_0, b_1, \dots, b_m)$  can be obtained through neural network training. At this point, the  $B$  matrix will correspondingly change to:

$$B = \begin{bmatrix} 0 \\ 0 \\ \vdots \\ \frac{1}{a_N} \end{bmatrix} [b_0 \quad b_1 \quad \dots \quad b_m] \quad (33)$$

However, there is a problem with equation 29: its state variables have  $n$  terms, while the right side of formula 25 has  $n + 1$  terms. To solve this problem, we can retain the  $x_1$  before iteration and append it to the state vector after iteration to obtain the complete  $n + 1$  state variables.

From this, we can obtain the output equation:

$$\tilde{\gamma} = aX \quad (34)$$

where  $a = (a_0, a_1, \dots, a_N)$ ,  $X = (x_1, x)^H$ .

Based on the above approach, we can obtain the calculation details of the FlightKooba method. As shown in Figure 2.

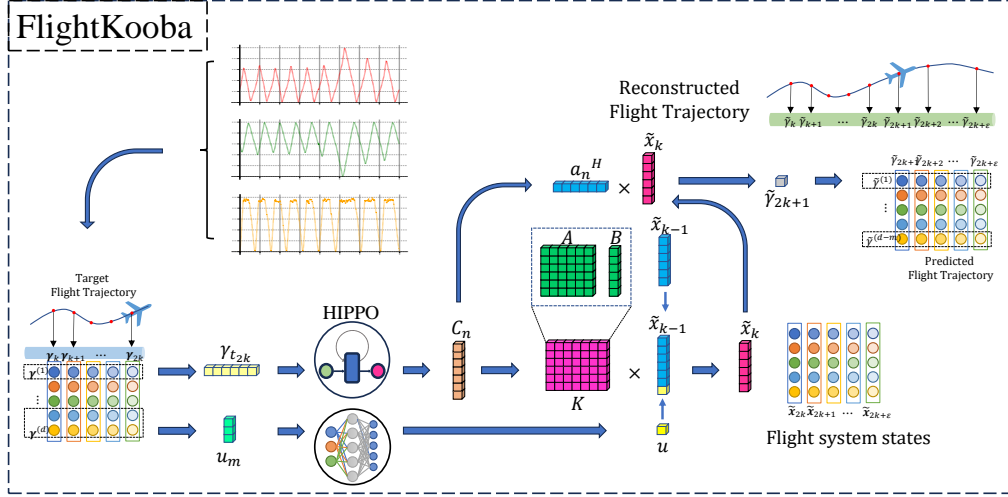


Figure 2: FlightKooba calculation details. The observation function is treated as a state equation and represented by Legendre polynomials. The coefficients of each polynomial are calculated using the HIPPO method, and these coefficients are then used to generate the Koopman operator, which can predict a series of future state changes.

The FlightKooba algorithm is described in the following algorithms 1.

---

#### Algorithm 1 FlightKooba Algorithm

---

**Input:** Data sequence  $\gamma_k$ , Control sequence  $u_k$ ;

**Output:** Prediction sequence  $\tilde{\gamma}_{k+\epsilon}$ ;

- 1: The data sequence  $\gamma_k$  is entered into the HIPPO block and the coefficients  $c_n$  are computed by iteratively;
  - 2: Generate the corresponding three matrices  $a_n$ ,  $A$ , and  $B$  based on the calculated coefficient  $c_n$ ;
  - 3: The matrix  $\mathcal{K}$  is generated by splicing the generated  $A$  and  $B$  matrices;
  - 4: The control sequence  $u_k$  is fed into FlightKooba and the coefficients  $b_m$  are calculated by back propagation;
  - 5: Iterative training is performed to compute the final  $b_m$ ;
  - 6: Calculate the future moment state  $\tilde{x}_{k+\epsilon}$  from matrix  $\mathcal{K}$  and the input future moment control sequence  $u_{k+\epsilon}$ ;
  - 7: Calculate the value of the future ( $\epsilon$  step) by  $\tilde{\gamma}_{k+\epsilon} = a_n * \tilde{x}_{k+\epsilon}$  to complete the prediction;
- return** Predicted value  $\tilde{\gamma}_{k+\epsilon}$
-

## 4. Data Overview

### 4.1. Flight Trajectory Dataset: CAFUC

The data set used in this work, named the Multidimensional Flight Trajectory Dataset of the Civil Aviation Flight University of China (CAFUC), from the real world, was generated from realistic fixed-wing aircraft flight training at CAFUC and contains 64 parameters, four artificial labels, 150,000 total frames, 41.6 h of total flight duration in CSV format, 14,356 basic maneuvers and 168 flight training subjects. However, it contains some features with text values or no change; after removing these features, 32 features are obtained that can be used for training. The CAFUC data set is available in the following repository: <https://github.com/CAFUC-JJJ/FlightKoopman>.

We have already provided a detailed introduction to this data set in our previous article [22], so we will not go into detail here.

### 4.2. Lorentz Attractor Dataset

The Lorenz attractor was discovered by American meteorologist Edward Lorenz in 1963 while solving a set of nonlinear ordinary differential equations. It is a mathematical model describing atmospheric convection and one of the most iconic examples of chaos theory.

The Lorenz attractor is described by the following set of ordinary differential equations:

$$\begin{cases} \frac{dx}{dt} = \sigma(y - x) \\ \frac{dy}{dt} = x(\rho - z) - y \\ \frac{dz}{dt} = xy - \beta z \end{cases} \quad (35)$$

Where  $x$ ,  $y$ , and  $z$  are system state variables, and  $\sigma$ ,  $\rho$ , and  $\beta$  are three constants.  $\sigma$ : Prandtl number, typically taken as a value around 10.  $\rho$ : Rayleigh Number, controls the convection intensity within the control system. 28 is a commonly used value in the Lorenz system. Under this parameter, the system exhibits typical chaotic behavior.  $\beta$ : Aspect Ratio, typically set to around 8/3, enabling the system to exhibit complex chaotic behavior. (This dataset is referred to as the Lorenz dataset in the subsequent experimental section.)

CAFUC and Lorenz datasets are primarily used for testing because they are related to physical systems. Similarly, to make the experiment more general, we will also test other classic time-series datasets.

### 4.3. Other Time Series Datasets

The following is a description of this data set: (1) Electricity [28] records electricity consumption data for 321 customers from 2012 to 2014. (2) ETT [35] consists of oil temperature and power load data recorded from power transformers between July 2016 and July 2018. (3) Exchange [1] contains daily exchange rate data for eight countries from 1990 to 2016. (4) ILI [24] includes weekly reported percentages of influenza-like illness cases from the US Centers for Disease Control and Prevention from 2002 to mid-2021. (5) Traffic [15] contains hourly road occupancy rate data for highways in the San Francisco Bay Area from January 2015 to December 2016. (6) Weather [36] is data on 21 weather indicators collected every 10 minutes by the Max Planck Institute for Biogeochemistry in 2020.

## 5. Experiments

In this section, we evaluate the performance of the FlightKooba module in predicting time series. Specifically, we will evaluate (a) the convergence speed of the algorithm on different datasets with randomly initialized parameters, (b) the model accuracy of FlightKooba compared to other methods on different datasets, and (c) the training time and memory usage on different datasets with the same hyperparameter settings.

In terms of modeling performance evaluation, we compared this method with two competing methods. (1) The latest results of the original xLSTM model by the LSTM team [3] (2) The Mamba module based on the state space model (SSM) [7]. It should be noted that the FlightKooba module is designed for a module in a neural network, so we will use the mamba module and the xLSTM module for comparison.

### 5.1. Overall Results

For each model: We set the number of modules for each model to 2, meaning that each model consists of two stacked blocks. The batch\_size is set to 32, and the seq\_len is set to 8 (owing to the large amount of electricity and transportation data, the seq\_len is set to 1 in both datasets to preserve the experimental results). We use the MSE loss function, the learning rate is set to 0.001, the number of epochs is set to 50, and we will evaluate the performance of each model by taking the average of 10 training runs.

For the data set: We process each data set based on the shape of the time series dataset (batch\_size, features, seq\_len). The first 70% of the entire data

set is used as the training set. Except for the CAFUC and Lorenz datasets, which use the remaining part as the test set, the other datasets are difficult to interpret due to large fluctuations in values, so only the last 200 data points of the training set are used as the test set. (All models mentioned in this article were tested on a Linux system equipped with an RTX 4080 SUPER graphics card.)

In terms of convergence speed, FlightKooba’s convergence speed is slightly insufficient, while Mamba and xLSTM both have good convergence speeds. In terms of prediction accuracy, the three models have different advantages in different datasets, and Mamba performs best overall. In terms of training time and memory usage, FlightKooba can match the training speed of the Mamba module without CUDA-level acceleration and is even faster on some datasets. The experimental results are summarized in Figure 3.

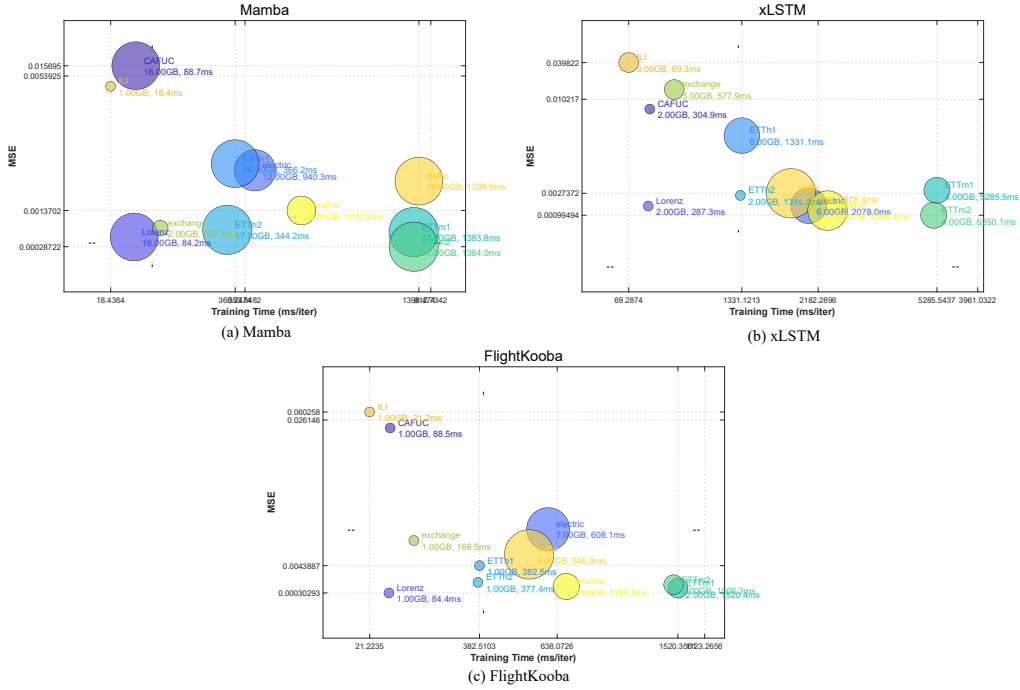


Figure 3: MSE-time-memory bubble plots for the three models across 11 datasets (a-c). Since the text in the figure is difficult to read, the table below provides all the detailed data in the figure. As shown in Table 1.

Since the text of the data in the plot is difficult to read, the following table gives all the data in the plot. As shown in Table 1.



Table 1: Overview of experimental results (training set).

Datasets	FlightKooba			Mamba			xLSTM		
	MSE	Times	Memory	MSE	Times	Memory	MSE	Times	Memory
CAFUC	0.0249	<b>88.54</b>	<b>1.00</b>	0.0157	88.70	16.00	<b>0.0094</b>	304.88	2.00
Lorenz	<b>0.0003</b>	84.44	<b>1.00</b>	0.0005	<b>84.15</b>	16.00	0.0017	287.31	2.00
Electricity	0.0098	<b>608.09</b>	7.00	0.0026	940.34	12.00	<b>0.0017</b>	2077.96	<b>6.00</b>
ETTh1	0.0043	382.51	<b>1.00</b>	<b>0.0028</b>	<b>366.25</b>	16.00	0.0073	1331.12	6.00
ETTh2	0.0018	377.40	<b>1.00</b>	<b>0.0008</b>	<b>344.24</b>	17.00	0.0026	1314.60	2.00
ETTm1	0.0010	1520.36	2.00	<b>0.0007</b>	<b>1383.79</b>	17.00	0.0030	5285.54	4.00
ETTm2	0.0015	1506.35	2.00	<b>0.0003</b>	<b>1384.00</b>	17.00	0.0010	5250.12	4.00
Exchange	0.0081	<b>166.48</b>	<b>1.00</b>	<b>0.0008</b>	157.06	2.00	0.0377	577.88	3.00
ILI	0.0602	21.22	<b>1.00</b>	<b>0.0050</b>	<b>18.44</b>	<b>1.00</b>	0.0398	69.29	3.00
Traffic	0.0060	<b>545.94</b>	9.00	<b>0.0022</b>	1398.47	16.00	0.0027	1878.39	10.00
Weather	<b>0.0012</b>	1153.25	3.00	0.0013	<b>1070.23</b>	6.00	0.0014	4065.36	7.00

The training time in the table is in *ms* and the memory is in *GB*. The experimental results show that FlightKooba currently performs well on datasets related to physical systems, but poorly on general time series datasets. In fact, this is one of the current shortcomings of FlightKooba. However, what is even more obvious is that FlightKooba has significant advantages in terms of time and memory.

In terms of model parameters, FlightKooba has the fewest parameters. The table 2 below shows the number of parameters for all models on different datasets.

Table 2: Total number of parameters of the model with different datasets.

datasets	FlightKooba	Mamba	xLSTM
CAFUC	12 / 1 120	12 992	22 434
Lorenz	3 / 38	936	3 254
Electricity	62 / 33 152	711 336	1 954 775
ETTh1	5 / 84	1 764	4 709
ETTh2	5 / 84	1 764	4 709
ETTm1	5 / 84	1 764	4 709
ETTm2	5 / 84	1 764	4 709
Exchange	5 / 126	2 064	5 226
ILI	4 / 120	1 764	4 709
Traffic	52 / 87 480	4 822 028	13 444 712
Weather	14 / 420	7 140	13 403

The data format of the FlightKooba column is (number of control items  $u$  / total number of parameters). Since FlightKooba requires support from control items  $u$ , but there are no control items in the dataset, we input the last  $k$  features into the model as control items  $u$  for training when using the FlightKooba module. This is also one of the reasons why the  $MSE$  value is relatively high in FlightKooba.

### 5.2. Convergence Rate

The experimental results for this section are shown in Figures 4 and 5. The Mamba module showed excellent convergence speed on different datasets, with very low loss values in the initial few epochs. xLSTM and FlightKooba performed similarly, with each having advantages on different datasets. It is worth noting that under the above parameter settings, the xLSTM model occasionally encountered a situation where the loss value became *nan* during training, which occurred more frequently after the learning rate changed to 0.003 (possibly due to a phenomenon known as gradient explosion).

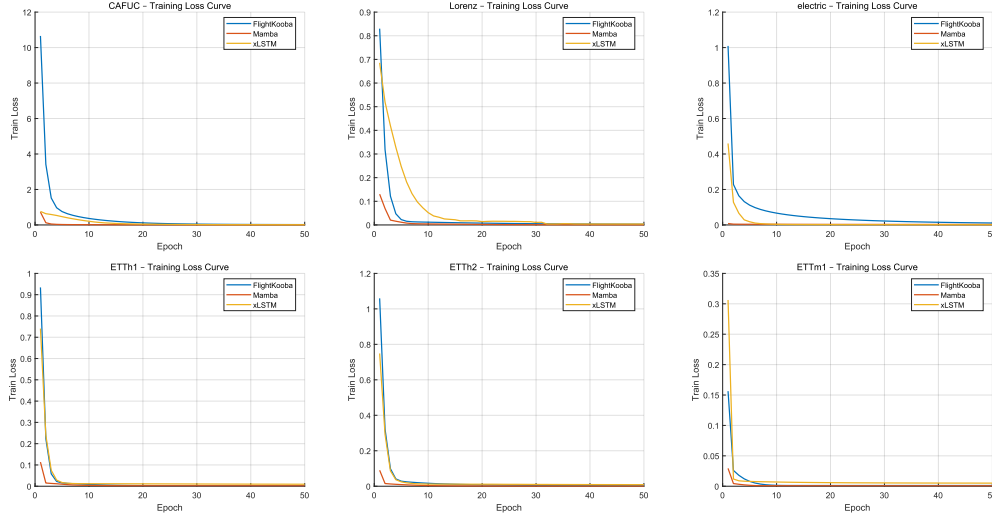


Figure 4: Convergence rate of each model on different training sets (a).

Overall, all three models converge quickly (loss values change dramatically only in the first 10 epochs on most datasets).

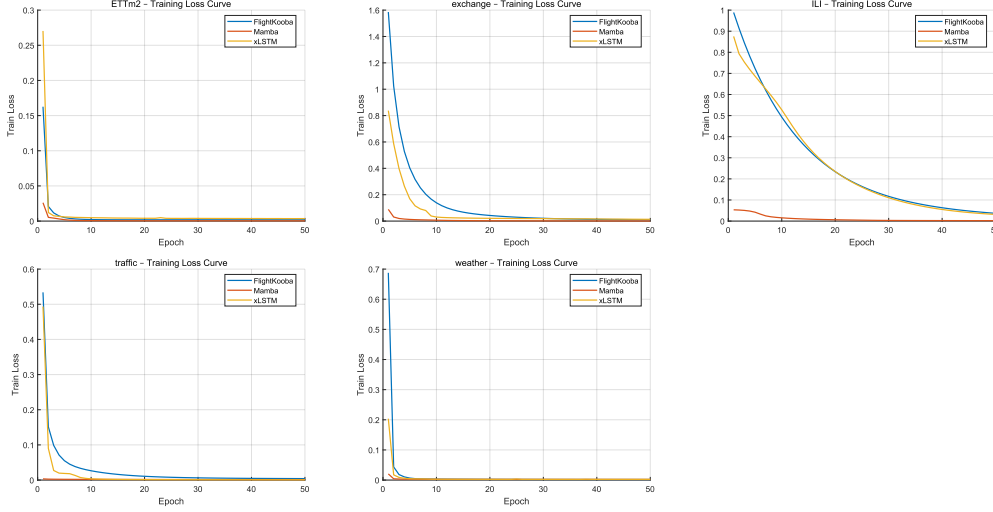


Figure 5: Convergence rate of each model on different training sets (b).

### 5.3. Accuracy

Due to the large number and high dimensionality of the datasets, it is not possible to provide predictions for all features in this section. Therefore, only one or two features from each dataset are shown in the test set. (Figures 6 and 7)

The prediction results show that each model performs differently on different datasets, and the same model also performs differently on different features within the same dataset. However, overall, the prediction results of each model are quite good. Among them, the Mamba model performs best in terms of comprehensive performance, while xLSTM and FlightKooba perform well and are not significantly different from each other.

Regarding the ablation experiment: In the FlightKooba structure, regardless of whether the matrix of the HIPPO module or the matrix of the Kooba module is replaced with a trainable parameter matrix, the results are poor, and the model has hardly learned any features of the system. This is because we derived the method for generating Koopman operators from the HIPPO method, which involves the calculation of factorials, making it difficult to learn trainable parameter matrices.

### 5.4. Summary And Analysis

In this section, we tested the performance of the FlightKooba, Mamba, and xLSTM modules on 11 datasets. Specifically, the performance of the

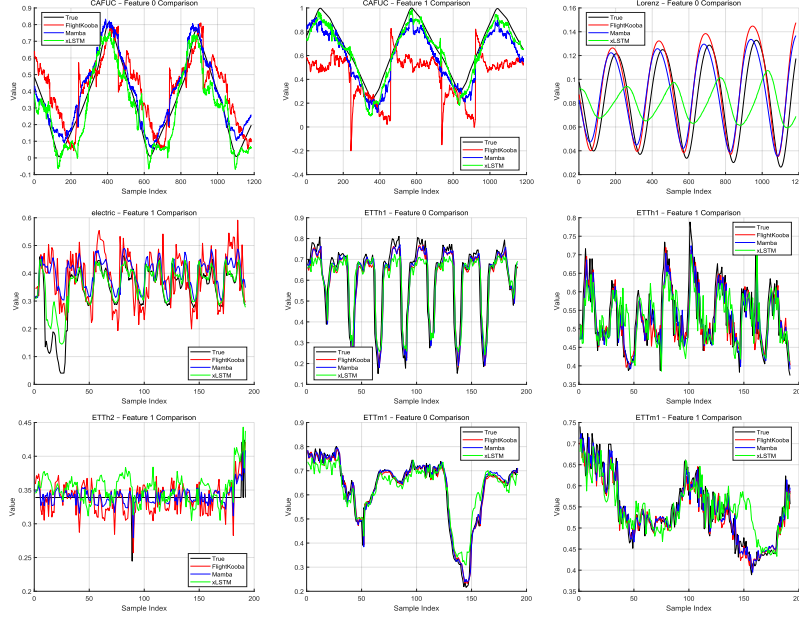


Figure 6: Selected prediction results for the three models on the test set for each dataset (a).

three models was compared in terms of convergence speed, accuracy, training time, and memory usage. The experimental results show that the FlightKooba module exhibits significant advantages in terms of training time, memory usage, and total number of parameters. Furthermore, the model accuracy achieved on the physical system dataset is on par with Mamba and xLSTM. This proves the feasibility of this calculation method, which makes it possible to introduce state space equations based on automatic control principles to construct and calculate Koopman operators.

Thanks to the SSM structure, Mamba and FlightKooba required less time for training. Compared to Mamba, FlightKooba uses state space equations to link the HIPPO method with Koopman theory, which is equivalent to determining the values of matrices  $A$ ,  $B$ , and  $C$  in the original SSM structure, further reducing the number of parameters that need to be calculated in the model.

However, FlightKooba performs poorly in certain situations. The following reasons are speculated: (a) The control variable  $u$  selected is not the precise control variable for the system, leading to a certain degree of deviation in the prediction results; (b) The approximation errors in the derivation

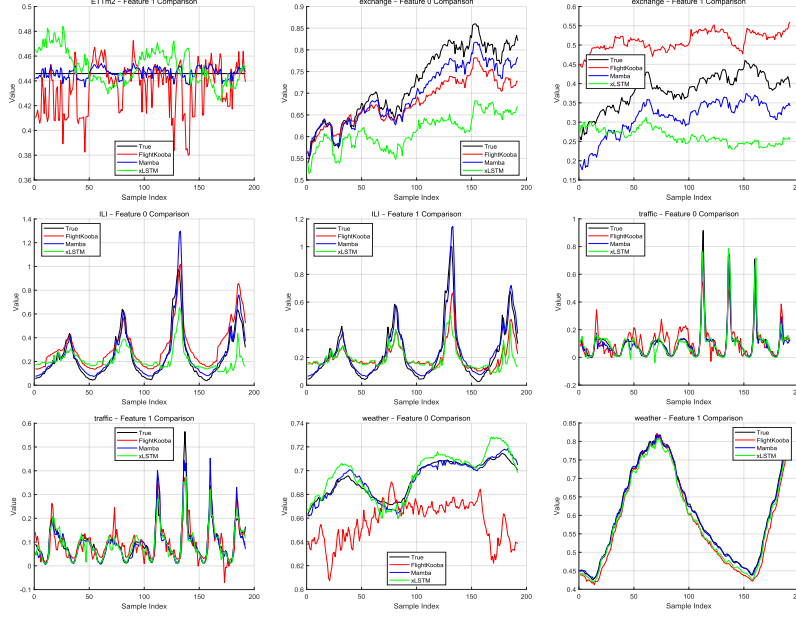


Figure 7: Selected prediction results for the three models on the test set for each dataset (b).

process affect the model to some extent; (c) The polynomial selected by the HIPPO method is a Legendre polynomial, which involves factorial calculations in the module, directly affecting the range of polynomial terms (the float type can only store factorial values up to approximately 32).

## 6. Conclusion And Future Works

In this paper, we propose a modeling and control framework based on the HIPPO method, Koopman theory, and state space equations from cybernetics: FlightKooba. This greatly improves the interpretability of the model and significantly reduces the number of trainable parameters. To evaluate the performance of FlightKooba, we tested and compared three models, FlightKooba, Mamba, and xLSTM, on multiple different datasets, including CAFUC and Lorenz. Experiments have demonstrated the superiority of the FlightKooba modeling method in terms of time and memory consumption (training time comparable to the Mamba module without CUDA-level acceleration; memory reduced by more than 50% on most datasets, with a tenfold reduction in the number of parameters), effectively completing the FTP task.

This provides a new method for the rapid calculation of Koopman operators, opening up new possibilities for the combination of time series prediction and control.

Similarly, in our experiment, we identified shortcomings that FlightKooba will need to address in the future:

- Other more suitable polynomials can be found to replace Legendre polynomials to fit the observed function, thereby eliminating the influence of factorials on the model.
- A unique physical acceleration algorithm can be constructed to further reduce the time required for model training and prediction.
- Modify the structure of FlightKooba to achieve higher accuracy in different physical systems (e.g., control variable  $u$  only affects the state vector, and interactions between different features are not reflected).

And applying the modeling framework based on FlightKooba to high-reliability intelligent aviation systems to support application scenarios for intelligent aviation management.

## Appendix A. Details of The HIPPO Algorithm

When we use models similar to RNN networks (including SSM) for learning, the output of each iteration is only related to the input and hidden layer state of the current step. The disadvantage is obvious: as time progresses, the historical information recorded by the model gradually decreases.

The HIPPO method was proposed to store data for a period of time using a finite-dimensional vector: the data for this period of time is regarded as a function  $\gamma(t)$ , which is approximated by a polynomial:

$$\gamma(t) = \sum_{i=0}^n c_n g_n(t) \quad (\text{A.1})$$

In this formula,  $g_n$  is a basis function with respect to time  $t$ , and  $c_n$  is the coefficient preceding each basis function. In this formula, we do not know the values of the coefficients  $c_n$ , which need to be calculated. For convenience of calculation, we specify that the basis functions  $g_n$  must satisfy the properties of standard orthogonal bases (the HIPPO method uses many types of orthogonal bases, and here we choose the normalized Legendre polynomials).

Referring to the idea of finding the coefficient  $c_n$  using Fourier series, we multiply both sides of A.1 by the conjugate  $g_n$  to obtain the formula for calculating the coefficient  $c_n$  (the domain of the normalized Legendre polynomial  $g_n$  is  $[-1, 1]$ ):

$$c_n = \int_{-1}^1 \gamma(t) g_n dt \quad (\text{A.2})$$

In order to make the above equation fit a more general time  $t \in [0, T]$ , find a mapping  $s \mapsto t \leq T(s)$  from  $[a, b]$  to  $[0, T]$  and then derive the coefficient calculation formula (In the HIPPO method, the mapping  $t \leq T(s) = (s + 1)\omega/2 + T - \omega$  used by *LegT* and the mapping used by *LegS* are  $t \leq T(s) = (s + 1)T/2$ ):

$$c_n = \int_a^b \gamma(t \leq T(s)) g_n(s) ds \quad (\text{A.3})$$

Then, differentiate both sides of A.3 and use integration by parts to obtain:

$$\begin{aligned} \frac{d}{dT} c_n(T) &= \gamma(t \leq T(s)) \left( \frac{\partial t \leq T(s)}{\partial T} / \frac{\partial t \leq T(s)}{\partial s} \right) \Big|_{s=b}^{s=a} g_n(s) \\ &\quad - \int_a^b \gamma(t \leq T(s)) d \left[ \left( \frac{\partial t \leq T(s)}{\partial T} / \frac{\partial t \leq T(s)}{\partial s} \right) g_n(s) \right] \end{aligned} \quad (\text{A.4})$$

The normalized Legendre polynomials  $g_n$  and the Legendre polynomials  $p_n$  are related by the following equation:

$$g_n(t) = \sqrt{\frac{2n+1}{2}} p_n(t) \quad (\text{A.5})$$

The Legendre polynomials and their derivatives are related by a recursive formula:

$$\frac{d}{dt} p_n(t) = n p_{n-1}(t) \quad (\text{A.6})$$

The idea behind *LegT* is basically the same as that behind *LegS*. Let us derive *LegT* below: Introduce a mapping  $t \leq T(s) = (s + 1)\omega/2 + T - \omega$ , which maps  $[-1, 1]$  to  $[T - \omega, T]$  (meaning that we only care about the history

of length  $\omega$ ), and then substitute it into equation A.4 to obtain:

$$\begin{aligned}
\frac{d}{dT}c_n(T) &= \gamma(t \leq T(s)) \left( \frac{\partial t \leq T(s)}{\partial T} / \frac{\partial t \leq T(s)}{\partial s} \right) g_n(s) \Big|_{s=-1}^{s=1} \\
&\quad - \int_{-1}^1 \gamma(t \leq T(s)) d \left[ \left( \frac{\partial t \leq T(s)}{\partial T} / \frac{\partial t \leq T(s)}{\partial s} \right) g_n(s) \right] \\
&= \sqrt{2(2n+1)} \left[ \frac{1}{\omega} \gamma(T) - (-1)^n \frac{1}{\omega} \gamma(T - \omega) \right] \\
&\quad - \int_{-1}^1 \gamma(t \leq T(s)) d \left[ \left( \frac{\partial t \leq T(s)}{\partial T} / \frac{\partial t \leq T(s)}{\partial s} \right) g_n(s) \right] \\
&= \sqrt{2(2n+1)} \left[ \frac{1}{\omega} \gamma(T) - (-1)^n \frac{1}{\omega} \gamma(T - \omega) \right] \\
&\quad - \frac{2}{\omega} \int_{-1}^1 \gamma(t \leq T(s)) g'_n(s) ds \\
&= \sqrt{2(2n+1)} \left[ \frac{1}{\omega} \gamma(T) - (-1)^n \frac{1}{\omega} \gamma(T - \omega) \right] \\
&\quad - \frac{2}{\omega} \int_{-1}^1 \gamma(t \leq T(s)) \sqrt{\frac{2n+1}{2}} p'_n(s) ds
\end{aligned} \tag{A.7}$$

To further solve this problem, another recursive formula from Legendre polynomials is used here:

$$p'_{n+1}(t) - p'_{n-1}(t) = (2n+1)p_n(t) \tag{A.8}$$

Expanding the above equation, we obtain:

$$\begin{aligned}
p'_{n+1}(t) &= (2n+1)p_n(t) + (2n-3)p_{n-2}(t) + \dots \\
&= \sum_{k=0}^n (2k+1) \tau_{n-k} p_k(t)
\end{aligned} \tag{A.9}$$

Among them, when  $k$  is even,  $\tau_{n-k} = 1$ ; otherwise,  $\tau_{n-k} = 0$ .



Therefore, equation A.7 can be further derived as follows:

$$\begin{aligned}
\frac{d}{dT}c_n(T) &= \sqrt{2(2n+1)} \left[ \frac{1}{\omega}\gamma(T) - (-1)^n \frac{1}{\omega}\gamma(T-\omega) \right] \\
&\quad - \frac{2}{\omega} \int_{-1}^1 \gamma(t \leq T(s)) \sqrt{\frac{2n+1}{2}} p_n'(s) ds \\
&= \sqrt{2(2n+1)} \left[ \frac{1}{\omega}\gamma(T) - (-1)^n \frac{1}{\omega}\gamma(T-\omega) \right] \\
&\quad - \frac{2}{\omega} \int_{-1}^1 \gamma(t \leq T(s)) \sqrt{\frac{2n+1}{2}} \sum_{k=0}^n (2k+1) \tau_{n-k-1} p_k(s) ds \\
&= \frac{\sqrt{2(2n+1)}}{\omega} [\gamma(T) - (-1)^n \gamma(T-\omega)] \\
&\quad - \frac{2}{\omega} \int_{-1}^1 \gamma(t \leq T(s)) \sqrt{\frac{2n+1}{2}} \sum_{k=0}^{n-1} \sqrt{2(2k+1)} \tau_{n-k-1} g_k(s) ds \\
&= \frac{\sqrt{2(2n+1)}}{\omega} [\gamma(T) - (-1)^n \gamma(T-\omega)] \\
&\quad - \frac{\sqrt{2(2n+1)}}{\omega} \int_{-1}^1 \gamma(t \leq T(s)) \sum_{k=0}^{n-1} \sqrt{2(2k+1)} \tau_{n-k-1} g_k(s) ds \\
&= \frac{\sqrt{2(2n+1)}}{\omega} [\gamma(T) - (-1)^n \gamma(T-\omega)] \\
&\quad - \frac{\sqrt{2(2n+1)}}{\omega} \sum_{k=0}^{n-1} \sqrt{2(2k+1)} \tau_{n-k-1} c_k(T) \tag{A.10}
\end{aligned}$$

From A.1 we obtain:

$$\gamma(t \leq T(s)) \approx \sum_{n=0}^N c_n g_n(s) \tag{A.11}$$

Let  $s = -1$ , we obtain:

$$\gamma(T-\omega) \approx \sum_{k=0}^N c_k g_k(-1) = \sum_{k=0}^N (-1)^k c_k(T) \sqrt{\frac{2k+1}{2}} \tag{A.12}$$

Substituting A.12 into A.10, we obtain:

$$\begin{aligned}
\frac{d}{dT}c_n(T) &= \frac{\sqrt{2(2n+1)}}{\omega}[\gamma(T) - (-1)^n\gamma(T-\omega)] \\
&\quad - \frac{\sqrt{2(2n+1)}}{\omega} \sum_{k=0}^{n-1} \sqrt{2(2k+1)}\tau_{n-k-1}c_k(T) \\
&= \frac{\sqrt{2(2n+1)}}{\omega}\gamma(T) - \frac{\sqrt{(2n+1)}}{\omega} \sum_{k=0}^N (-1)^{n-k}c_k(T)\sqrt{2k+1} \\
&\quad - \frac{\sqrt{2n+1}}{\omega} \sum_{k=0}^{n-1} \sqrt{(2k+1)}2\tau_{n-k-1}c_k(T) \\
&= \frac{\sqrt{2(2n+1)}}{\omega}\gamma(T) - \frac{\sqrt{(2n+1)}}{\omega} \sum_{k=n}^N (-1)^{n-k}c_k(T)\sqrt{2k+1} \\
&\quad - \frac{\sqrt{2n+1}}{\omega} \sum_{k=0}^{n-1} \sqrt{(2k+1)}(2\tau_{n-k-1} + (-1)^{n-k})c_k(T) \quad (\text{A.13})
\end{aligned}$$

Among these,  $2\tau_{n-k-1} + (-1)^{n-k}$  represents the number of terms used in the polynomial approximation of  $\gamma(t)$ . Therefore, we can choose  $n$  to be an even number, i.e., use an even number of terms for the approximation. Based on this,  $n-k-1$  and  $n-k$  must be one odd and one even number. When  $n-k$  is even,  $k$  is even, then  $2\tau_{n-k-1} = 0$  and  $(-1)^{n-k} = 1$ ; when  $n-k$  is odd,  $k$  is odd, then  $2\tau_{n-k-1} = 2$  and  $(-1)^{n-k} = -1$ . That is,  $2\tau_{n-k-1} + (-1)^{n-k} \equiv 1$ . Therefore, Equation A.13 can be simplified to:

$$\begin{aligned}
\frac{d}{dT}c_n(T) &= \frac{\sqrt{2(2n+1)}}{\omega}\gamma(T) - \frac{\sqrt{(2n+1)}}{\omega} \sum_{k=n}^N (-1)^{n-k}c_k(T)\sqrt{2k+1} \\
&\quad - \frac{\sqrt{2n+1}}{\omega} \sum_{k=0}^{n-1} \sqrt{(2k+1)}c_k(T) \quad (\text{A.14})
\end{aligned}$$

The above equation can be converted into matrix form:

$$c'(t) = Nc(t) + M\gamma(t) \quad (\text{A.15})$$

Among them,  $c(t) = [c_0(T), c_1(T), \dots, c_N(T)]$ , and the expressions of matrices  $N$  and  $M$  are as follows:

$$N_{n,k} = -\frac{1}{\omega} \begin{cases} \sqrt{(2n+1)(2k+1)}, & k < n \\ (-1)^{n-k}\sqrt{(2n+1)(2k+1)}, & k \geq n \end{cases} \quad (\text{A.16})$$

$$M_n = \frac{1}{\omega} \sqrt{2(2n+1)} \quad (\text{A.17})$$

Introducing the scaling factor  $\lambda_n = \frac{2}{\sqrt{2n+1}}$ , such that  $c_n(T) = \lambda_n \tilde{c}_n(T)$ , the expressions for matrices  $N$  and  $M$  become:

$$N_{n,k} = -\frac{1}{\omega} \begin{cases} 2n+1, & k < n \\ (-1)^{n-k}(2n+1), & k \geq n \end{cases} \quad (\text{A.18})$$

$$M_n = \frac{1}{\omega} (2n+1) \quad (\text{A.19})$$

Following the same line of reasoning, introducing the mapping  $t \leq T(s) = (s+1)T/2$  and the scaling factor  $\lambda_n = \sqrt{2}$ , we obtain the expressions for the LegS method matrices  $N$  and  $M$ :

$$N_{n,k} = \begin{cases} \sqrt{(2n+1)(2k+1)}, & k < n \\ n+1, & k = n \\ 0, & k > n \end{cases} \quad (\text{A.20})$$

$$M_n = \sqrt{2(2n+1)} \quad (\text{A.21})$$

## Appendix B. Multi-step Iteration

To facilitate iterative solution with a computer, equation A.15 is discretized. First, the left side of the equation is handled by approximating  $c'(t)$  in continuous time as the slope between two points  $c_{t_{k+1}}$  and  $c_{t_k}$ , i.e.,:

$$\dot{c}(t_k) \approx \frac{c_{t_{k+1}} - c_{t_k}}{\Delta t} \quad (\text{B.1})$$

Then, we move on to the discretization on the right side of the equation. Since the data we obtain is discrete, we assume that  $\gamma(t)$  is a fixed value between  $[t_k, t_{k+1}]$ , so we can discretize  $\gamma(t)$  as  $\gamma_k = \gamma(t_k)$ . There are two ways to discretize  $c(t)$ . One assumes that  $c_{t_k} = c(t_k)$  in the interval  $[t_k, t_{k+1}]$ , and the other assumes that  $c_{t_{k+1}} = c(t_k)$ , i.e., the two values at the endpoints of the interval. If we consider  $c_{t_k} = c(t_k)$ , we obtain:

$$\frac{c_{t_{k+1}} - c_{t_k}}{\Delta t} = N c_{t_k} + M \gamma_k \quad (\text{B.2})$$

After simplifying the equation, we obtain:

$$c_{t_{k+1}} = (I + \Delta t N) c_{t_k} + \Delta t M \gamma_k \quad (\text{B.3})$$

At this point, if we consider  $c_{t_{k+1}} = c(t_k)$ , we obtain:

$$\frac{c_{t_{k+1}} - c_{t_k}}{\Delta t} = N c_{t_{k+1}} + M \gamma_k \quad (\text{B.4})$$

After simplifying the equation, we obtain:

$$c_{t_{k+1}} = (I - \Delta t N)^{-1} (c_{t_k} + \Delta t M \gamma_k) \quad (\text{B.5})$$

With the above two equations B.3 and B.5, a third method for estimating the value of  $c(t_k)$  emerges, which assumes that:

$$\frac{1}{2} (c_{t_{k+1}} + c_{t_k}) = c(t_k) \quad (\text{B.6})$$

This approximate estimation method is more reasonable than either of the previous two methods, i.e., the frequently mentioned bilinear form. Substituting equation B.6 into equation B.2 yields:

$$\frac{c_{t_{k+1}} - c_{t_k}}{\Delta t} = N \frac{1}{2} (c_{t_k} + c_{t_{k+1}}) + M \gamma_k \quad (\text{B.7})$$

After sorting, we get:

$$c_{t_{k+1}} = \left( I - \frac{\Delta t}{2} N \right)^{-1} \left[ \left( I + \frac{\Delta t}{2} N \right) c_{t_k} + \Delta t M \gamma_k \right] \quad (\text{B.8})$$

Here,  $\Delta t$  is a hyperparameter representing the distance between discrete points, also known as step size.

Therefore, equation A.15 is discretized as follows:

$$c_{t_{k+1}} = \overline{N} c_{t_k} + \overline{M} \gamma_k \quad (\text{B.9})$$

Among them, the expressions of matrices  $\overline{N}$  and  $\overline{M}$  are as follows:

$$\overline{N} = \left( I - \frac{\Delta t}{2} N \right)^{-1} \left( I + \frac{\Delta t}{2} N \right) \quad (\text{B.10})$$

$$\overline{M} = \Delta t \left( I - \frac{\Delta t}{2} N \right)^{-1} M \quad (\text{B.11})$$

Next, we will consider how to perform batch training on equation B.9. Starting from  $k = 1$  and setting the initial state  $c_{t_1} = 0$ , we have:

$$c_{t_2} = \overline{M}\gamma_1 \quad (\text{B.12})$$

$$c_{t_3} = \overline{N}\overline{M}\gamma_1 + \overline{M}\gamma_2 \quad (\text{B.13})$$

$$c_{t_4} = \overline{N}\overline{N}\overline{M}\gamma_1 + \overline{N}\overline{M}\gamma_2 + \overline{M}\gamma_3 \quad (\text{B.14})$$

...

$$c_{t_{k+1}} = \overline{N}^{k-1}\overline{M}\gamma_1 + \overline{N}^{k-2}\overline{M}\gamma_2 + \dots + \overline{N}\overline{M}\gamma_{k-1} + \overline{M}\gamma_k \quad (\text{B.15})$$

For convenience of derivation, we write  $c_{t_{k+1}}$  in matrix form:

$$\begin{aligned} c_{t_{k+1}} &= \overline{N}^{k-1}\overline{M}\gamma_1 + \overline{N}^{k-2}\overline{M}\gamma_2 + \dots + \overline{N}\overline{M}\gamma_{k-1} + \overline{M}\gamma_k \\ &= (\overline{N}^{k-1}, \overline{N}^{k-2}, \dots, \overline{N}, I)\overline{M}\gamma(t_k) \\ &= R\overline{M}\gamma(t_k) \end{aligned} \quad (\text{B.16})$$

where  $R = (\overline{N}^{k-1}, \overline{N}^{k-2}, \dots, \overline{N}, I)$ ,  $\overline{M} = \Delta t \left( I - \frac{\Delta t}{2} N \right)^{-1} M$ .  $\gamma(t_k) = (\gamma_1, \gamma_2, \dots, \gamma_k)^T$  denotes the observed values of  $\gamma(t)$  from  $\gamma_k$  backward to the discrete values  $k-1$  to the discrete value  $k$ th (a total of values  $k$ , i.e. a total of  $k$  iterations).

When continuing training,  $c_{t_{k+1}}$  is a non-zero value, so we need to obtain a more general iterative formula. Continuing with the above approach, we obtain:

$$c_{t_{2k+1}} = \overline{N}^{k-1}\overline{M}\gamma_k + \overline{N}^{k-2}\overline{M}\gamma_{k+1} + \dots + \overline{N}\overline{M}\gamma_{2k-1} + \overline{M}\gamma_{2k} \quad (\text{B.17})$$

It can also be written in matrix form similar to B.16:

$$c_{t_{2k+1}} = \overline{N}^{k-1}c_{t_k} + R\overline{M}\gamma(t_{2k}) \quad (\text{B.18})$$

Therefore, during the actual iteration, it is only necessary to calculate the  $k-1$ th power of the matrix once and store the result, which can then be used until the iteration ends, thereby reducing the time complexity of the algorithm.

## References

- [1] Abedin, M. Z., Moon, M. H., Hassan, M. K., & Hajek, P. (2025). Deep learning-based exchange rate prediction during the covid-19 pandemic. *Annals of Operations Research*, *345*, 1335–1386. doi:<https://doi.org/10.1007/s10479-021-04420-6>.
- [2] Arbabi, H., & Mezic, I. (2017). Ergodic theory, dynamic mode decomposition, and computation of spectral properties of the koopman operator. *SIAM Journal on Applied Dynamical Systems*, *16*, 2096–2126. doi:<https://doi.org/10.1137/17M1125236>.
- [3] Beck, M., Pöppel, K., Spanring, M., Auer, A., Prudnikova, O., Kopp, M., Klambauer, G., Brandstetter, J., & Hochreiter, S. (2024). xlstm: Extended long short-term memory. *arXiv preprint arXiv:2405.04517*, . doi:<https://doi.org/10.48550/arXiv.2405.04517>.
- [4] Budalakoti, S., Srivastava, A., & Otey, M. (2009). Anomaly detection and diagnosis algorithms for discrete symbol sequences with applications to airline safety. *IEEE Transactions on Systems, Man, and Cybernetics, Part C (Applications and Reviews)*, *39*, 101–113. doi:[10.1109/TSMCC.2008.2007248](https://doi.org/10.1109/TSMCC.2008.2007248).
- [5] Chen, H., & Lv, C. (2024). Incorporating eso into deep koopman operator modeling for control of autonomous vehicles. *IEEE Transactions on Control Systems Technology*, . doi:[10.1109/TCST.2024.3378456](https://doi.org/10.1109/TCST.2024.3378456).
- [6] Gavrilovski, A., Jimenez, H., Mavris, D. N., Rao, A. H., Shin, S., Hwang, I., & Marais, K. (2016). Challenges and opportunities in flight data mining: A review of the state of the art. *AIAA Infotech@ Aerospace*, (p. 0923). doi:<https://doi.org/10.2514/6.2016-0923>.
- [7] Gu, A., & Dao, T. (2023). Mamba: Linear-time sequence modeling with selective state spaces. *arXiv preprint arXiv:2312.00752*, . doi:<https://doi.org/10.48550/arXiv.2312.00752>.
- [8] Gu, A., Dao, T., Ermon, S., Rudra, A., & Ré, C. (2020). Hippo: Recurrent memory with optimal polynomial projections. *Advances in neural information processing systems*, *33*, 1474–1487. doi:<https://doi.org/10.48550/arXiv.2008.07669>.

- [9] Gu, A., Goel, K., & Ré, C. (2021). Efficiently modeling long sequences with structured state spaces. *arXiv preprint arXiv:2111.00396*, . doi:<https://doi.org/10.48550/arXiv.2111.00396>.
- [10] Ha, D., & Schmidhuber, J. (2018). World models. *arXiv preprint arXiv:1803.10122*, . doi:<https://doi.org/10.5281/zenodo.1207631>.
- [11] Hafner, D., Lillicrap, T., Ba, J., & Norouzi, M. (2019). Dream to control: Learning behaviors by latent imagination. *arXiv preprint arXiv:1912.01603*, . doi:<https://doi.org/10.48550/arXiv.1912.01603>.
- [12] Hafner, D., Lillicrap, T., Norouzi, M., & Ba, J. (2020). Mastering atari with discrete world models. *arXiv preprint arXiv:2010.02193*, . doi:<https://doi.org/10.48550/arXiv.2010.02193>.
- [13] Hafner, D., Pasukonis, J., Ba, J., & Lillicrap, T. (2023). Mastering diverse domains through world models. *arXiv preprint arXiv:2301.04104*, . doi:<https://doi.org/10.48550/arXiv.2301.04104>.
- [14] Han, M., Euler-Rolle, J., & Katzschmann, R. K. (2022). Desko: Stability-assured robust control with a deep stochastic koopman operator. In *International conference on learning representations (ICLR)*. doi:<https://doi.org/10.3929/ethz-b-000694283>.
- [15] Harrou, F., Zeroual, A., Kadri, F., & Sun, Y. (2024). Enhancing road traffic flow prediction with improved deep learning using wavelet transforms. *Results in Engineering*, 23, 102342. doi:<https://doi.org/10.1016/j.rineng.2024.102342>.
- [16] Kalman, R. E. (1960). A new approach to linear filtering and prediction problems, . doi:<https://doi.org/10.1115/1.3662552>.
- [17] Koopman, B. O. (1931). Hamiltonian systems and transformation in hilbert space. *Proceedings of the National Academy of Sciences*, 17, 315–318. doi:<https://doi.org/10.1073/pnas.17.5.315>.
- [18] Korda, M., & Mezić, I. (2018). Linear predictors for nonlinear dynamical systems: Koopman operator meets model predictive control. *Automatica*, 93, 149–160. doi:<https://doi.org/10.1016/j.automatica.2018.03.046>.

- [19] Li, F., Feng, J., Yan, H., Jin, G., Yang, F., Sun, F., Jin, D., & Li, Y. (2023). Dynamic graph convolutional recurrent network for traffic prediction: Benchmark and solution. *ACM Transactions on Knowledge Discovery from Data*, 17, 1–21. doi:<https://doi.org/10.1145/3532611>.
- [20] Li, Y., He, H., Wu, J., Katabi, D., & Torralba, A. (2019). Learning compositional koopman operators for model-based control. *arXiv preprint arXiv:1910.08264*, . doi:<https://doi.org/10.48550/arXiv.1910.08264>.
- [21] Li, Z., Han, M., & Yin, X. (2025). Mamko: Mamba-based koopman operator for modeling and predictive control. In *The Thirteenth International Conference on Learning Representations*.
- [22] Lu, J., Jiang, J., Bai, Y., Dai, W., & Zhang, W. (2025). Flightkoopman: Deep koopman for multi-dimensional flight trajectory prediction. *International Journal of Computational Intelligence and Applications*, (p. 2450038). doi:<https://doi.org/10.1142/S146902682450038X>.
- [23] Morton, J., Jameson, A., Kochenderfer, M. J., & Witherden, F. (2018). Deep dynamical modeling and control of unsteady fluid flows. *Advances in Neural Information Processing Systems*, 31. doi:<https://doi.org/10.48550/arXiv.1805.07472>.
- [24] Peng, B., Ding, Y., & Kang, W. (2023). Metaformer: a transformer that tends to mine metaphorical-level information. *Sensors*, 23, 5093. doi:<https://doi.org/10.3390/s23115093>.
- [25] Schmid, P. J. (2010). Dynamic mode decomposition of numerical and experimental data. *Journal of fluid mechanics*, 656, 5–28. doi:<https://doi.org/10.1017/S0022112010001217>.
- [26] Schulze, J. C., Doncevic, D. T., & Mitsos, A. (2022). Identification of mimo wiener-type koopman models for data-driven model reduction using deep learning. *Computers & Chemical Engineering*, 161, 107781. doi:<https://doi.org/10.1016/j.compchemeng.2022.107781>.
- [27] Shi, H., & Meng, M. Q.-H. (2022). Deep koopman operator with control for nonlinear systems. *IEEE Robotics and Automation Letters*, 7, 7700–7707. doi:[10.1109/LRA.2022.3184036](https://doi.org/10.1109/LRA.2022.3184036).



- [28] Velasco, L. C. P., Arnejo, K. A. S., & Macarat, J. S. S. (2022). Performance analysis of artificial neural network models for hour-ahead electric load forecasting. *Procedia Computer Science*, 197, 16–24. doi:<https://doi.org/10.1016/j.procs.2021.12.113>.
- [29] Verma, Y., Heinonen, M., & Garg, V. (). Climode: Climate and weather forecasting with physics-informed neural odes, 2024. URL <https://arxiv.org/abs/2404.10024>, . doi:<https://doi.org/10.48550/arXiv.2404.10024>.
- [30] Wang, K., Wu, H., Duan, Y., Zhang, G., Wang, K., Peng, X., Zheng, Y., Liang, Y., & Wang, Y. (2024). Nuwadynamics: Discovering and updating in causal spatio-temporal modeling. In *The Twelfth International Conference on Learning Representations*.
- [31] Williams, M. O., Kevrekidis, I. G., & Rowley, C. W. (2015). A data-driven approximation of the koopman operator: Extending dynamic mode decomposition. *Journal of Nonlinear Science*, 25, 1307–1346. doi:<https://doi.org/10.1007/s00332-015-9258-5>.
- [32] Williams, M. O., Kevrekidis, I. G., & Rowley, C. W. (2015). A data-driven approximation of the koopman operator: Extending dynamic mode decomposition. *Journal of Nonlinear Science*, 25, 1307–1346. doi:<https://doi.org/10.1007/s00332-015-9258-5>.
- [33] Zeng, W., Chu, X., Xu, Z., Liu, Y., & Quan, Z. (2022). Aircraft 4d trajectory prediction in civil aviation: a review. *aerospace* 9 (2): 91. doi:<https://doi.org/10.3390/aerospace9020091>.
- [34] Zhang, X., Han, M., & Yin, X. (2023). Reduced-order koopman modeling and predictive control of nonlinear processes. *Computers & Chemical Engineering*, 179, 108440. doi:<https://doi.org/10.1016/j.compchemeng.2023.108440>.
- [35] Zhou, H., Zhang, S., Peng, J., Zhang, S., Li, J., Xiong, H., & Zhang, W. (2021). Informer: Beyond efficient transformer for long sequence time-series forecasting. In *Proceedings of the AAAI conference on artificial intelligence* (pp. 11106–11115). volume 35. doi:<https://doi.org/10.1609/aaai.v35i12.17325>.
- [36] Zuo, H.-M., Qiu, J., Jia, Y.-H., Wang, Q., & Li, F.-F. (2022). Ten-minute prediction of solar irradiance based on cloud detection and a

long short-term memory (lstm) model. *Energy Reports*, 8, 5146–5157.  
doi:<https://doi.org/10.1016/j.egy.2022.03.182>.